Geometry optimisation of highly crowned gear couplings working in high misalignment applications to reduce tooth root stresses

Aurea Iñurritegui[1], *Jon* Larrañaga[1], *Aitor* Arana[1], and *Ibai* Ulacia[1,*]

[1]Mondragon Unibertsitatea, Faculty of Engineering, Loramendi 4, 20500 Mondragon, Spain

Abstract. Crowned gear couplings are mechanical components used to transmit power between misaligned rotating shafts. Their geometry is characterised by a significant longitudinal crowning to accommodate angular misalignment. Recent studies reveal that high misalignments drastically reduce the number of teeth in contact and lead to an uneven load distribution among engaged teeth. Consequently, tooth root fracture becomes a common failure mode. Current standards only address misalignment angles below 1.5°, treating applications with greater misalignments as special cases without design guidelines or stress prediction methods. This study proposes a procedure to optimize the design of crowned gear couplings working in high misalignment applications by determining tooth root stress distribution. The geometry is analytically generated, while finite element models are used to calculate the stress distribution. Experimental validation is performed using a dedicated test rig. The obtained results are very close to the ones from the numerical model, demonstrating the suitability of the method for crowned gear couplings operating under significant angular misalignments. The optimized design reduces tooth root stress by 50%, which will increase the fatigue life of the component or enable the application of higher torque values.

1 Introduction

Gear couplings are used to transmit power between shafts due to their high-power density compared to other non-splined connections [1]. Crowned spherical gear couplings are specially designed to work with high misalignment angles ($\gamma \gg 1°$). These couplings require active surfaces with a large amount of longitudinal crowning to obtain a favourable contact pattern under high misalignment conditions ($3° \leq \gamma \leq 10°$). In addition, this longitudinal crowning prevents the teeth from interference with the sleeve during operation and balances the clearance between the hub and sleeve, while increasing the contact ratio [2]. However, the large amount of longitudinal crowning (≫100 μm), coupled with the small tool path radius used in its manufacture, poses challenges when analytically generating the surfaces of crowned gear couplings. One of the most significant is the appearance of singularities (corresponding to undercut sections). For this reason, an analytical generation model that takes into account the thread surface of the hob during generation has recently been developed [3] and experimentally validated [4]. This model has advantages over other published models [5,6], because it is able to generate tooth surfaces with a large amount of crowning and to produce undercut sections. Moreover, none of the models present in the literature were experimentally validated, as is the case of the proposed model [4].

The gear couplings must have a specific amount of backlash to avoid interference and, at the same time, enable the angular misalignment [6-9]. Angular clearance is the angle of rotation that exists when rotating the teeth on the hub while keeping the sleeve stationary, i.e. from the point where the left flanks are in contact to the point where the right flanks are in contact [7,10]. Since the tooth surface is crowned and there is angular misalignment, the value of the clearance will not be constant for all teeth [2,11]. Indeed, the tilting angular pitch positions will have a smaller clearance than those on the pivoting position, resulting in a progressive contact of the teeth [12]. Thus, the teeth in the tilting position are the first to come into contact and will experience the greatest tooth root stresses [13,14]. In addition, the uneven clearance distribution will cause the number of teeth in contact to vary as a function of the applied torque and misalignment angle, resulting in a variation of the coupling stiffness [15]. To determine the number of teeth in contact, the scientific literature shows finite element models [16,17] and unloaded tooth contact analysis algorithms [3,18]. However, the standards [7,9,19,20] do not include the effect of geometry or loading conditions in their equations. That is, they define the percentage of the number of teeth in contact only as a function of the misalignment angle, without taking into account their stiffness and applied torque. For this reason, it is a common criterion to consider that half of the coupling teeth will be in contact [7-9,19]. This criterion may be adequate in applications with small angular

* Corresponding author: iulacia@mondragon.edu

© The Authors, published by EDP Sciences. This is an open access article distributed under the terms of the Creative Commons Attribution License 4.0 (https://creativecommons.org/licenses/by/4.0/).

misalignments ($\gamma \gg 1°$), however, finite element models [17,21] have shown that it is not extensible for applications with high misalignment. The main reason is that the number of teeth in contact can be even less than the half, especially in low load and high misalignment applications. This fact was demonstrated numerically [17] and experimentally [4].

Since gear couplings are frequently used in applications with small misalignment angles [14,22], most experimental studies and test rigs are oriented towards these working conditions [23,24]. The conducted studies have demonstrated that the contact pattern is not centred nor maintained constant under misalignment conditions [6,25], and wear increases with the misalignment angle [26]. However, Mancuso [27] demonstrated that common failures in couplings operating under heavy applications with up to $\gamma = 6°$ are more related to tooth root fractures, highlighting that the misalignment angle was the most detrimental variable.

Regarding conditions with misalignment, and considering the importance of the misalignment angle, there are analytical studies that have determined the relationship between the design parameters of the gear coupling and the maximum achievable misalignment angle [28], showing values very close to reality experimental analysis [4]. It has also been concluded that the number of teeth and the pressure angle are the predominant design parameters, followed by the crowning radius to define the maximum misalignment at which a crowned gear coupling can operate. Experimental studies, on the other hand, are more limited. For example, Herbstritt et al. [29] measured stresses at the tooth root with a maximum misalignment angle of $\gamma = 3°$ and validated a finite element model with a 15% margin of error. However, there was limited information about the experimental methodology. More recently, Inurritegui et al. [4] presented a test rig where tests were conducted up to an angular misalignment of 10°. In this work, they also validated the number of teeth in contact, the contact pattern, and the stiffness of a coupling up to a misalignment of 7° with an error below 15%. However, there was no information regarding tooth root stress values in this case.

The literature has demonstrated that crowned gear couplings pose a series of challenges in terms of geometry and mechanical behaviour. Moreover, current standards still consider them as exceptional cases and do not provide precise sizing criteria. Recently, significant advancements have been made in the development of analytical and finite element models to determine the geometry of tooth surfaces and the mechanical behaviour of crowned gear couplings. However, a clear methodology for the design and sizing of couplings based on tooth root fracture criteria is still lacking. Therefore, the main objective of this study is to present the tools and methodology to be employed in designing and optimizing a crowned ger coupling that currently operates under high misalignment conditions, while also experimentally validating the stress distribution at the tooth root.

2 Methodology

In this section, a brief summary is provided of the analytical and numerical models that will be used for the design and sizing of gear couplings in this study. The case study employed is the gear coupling used in the rolling mill for high-strength steel. The high number of rolls in a reduced space, combined with the use of large gearboxes, results in a very high misalignment angle between the rolls and the gearbox, reaching angles greater than 6° [21,31]. The design conditions for this application are detailed in Table 1. It should be noted that the maximum applied torque corresponds to the central rolls operating under nearly aligned conditions. The applied torque on the outer rolls, that is, the most misaligned ones, decreases to approximately half (500 Nm).

Table 1. Design and operating conditions of the gear couplings in the rolling mill.

Parameter	Value	Unit
Maximum pitch diameter	50	mm
Maximum misalignment	6	º
Maximum torque	1000	Nm

The geometrical parameters of the gear couplings currently used in the rolling mill and which will be used for the experimental validation are listed in Table 2. The material from which they have been manufactured is a carburised and hardened 15NiCr11 steel with the mechanical properties set out in Table 2.

Table 2. Geometry parameters of the case study (Current case) employed on the rolling machine and material properties.

Parameter	Value	Unit
Pitch diameter	39	mm
Normal module	3	mm
Number of teeth	13	-
Pressure angle	30	º
Aspect ratio	0.30	-
Normal clearance	0.285	mm
Crowning radius	10	mm
Young modulus	210	GPa
Poisson coefficient	0.33	-
Density	7850	kg/m^3
Elastic modulus	850	MPa

2.1 Analytical geometry generation model

To analyse the mechanical behaviour and geometric characteristics of gear couplings, it is necessary to generate the geometry analytically. This involves considering both the manufacturing process and the geometry of the cutting tool. In the case of the hub, the hobbing process with a circular tool path and the generating gear hob, respectively, are taken into account. For the sleeve, the generating process using a shaper cutter and the shaper cutter itself are considered.

The spherical surfaces of the hub teeth are generated by considering the thread surface of the hob cutter as a set of cutting edges that act simultaneously during the generation process, as explained in [3]. This is a two-

parameter envelope generation process [30], where the thread surface of the hob cutter is determined prior to the generation of the hub.

First, the thread surface of the hob cutter (Σ_w) is generated as the cutting tool based on the rack cutter tooth surface (Σ_c). The hob cutter follows a circular feed motion that determines the shaft tooth surface (Σ_h) as the envelope to the family of hob cutter surfaces. The thread surface of the hob cutter is determined from the rack tooth surface Σ_c by considering the meshing equation (2). The hub tooth surface is generated by coordinate transformation (1) from the coordinate system S_c to the coordinate system S_h, taking into account the double enveloping process [30] with two independent generation parameters ϕ_w and s_w ((3), (4)).

$$r_h(u, v, \psi_w, s_w, \phi_w) = \mathbf{M}_{hw}\,\mathbf{M}_{wc}\,\mathbf{r}_c(u, v) \quad (1)$$

$$f_1(u, v, \psi_w) = \left(\frac{\partial \mathbf{r}_w}{\partial u} \times \frac{\partial \mathbf{r}_w}{\partial v}\right)\frac{\partial \mathbf{r}_w}{\partial \psi_w} \quad (2)$$

$$f_2(u, v, s_w, \phi_w) = \left(\frac{\partial \mathbf{r}_h}{\partial u} \times \frac{\partial \mathbf{r}_h}{\partial v}\right)\frac{\partial \mathbf{r}_h}{\partial \phi_w} \quad (3)$$

$$f_3(u, v, s_w, \phi_w) = \left(\frac{\partial \mathbf{r}_h}{\partial u} \times \frac{\partial \mathbf{r}_h}{\partial v}\right)\frac{\partial \mathbf{r}_h}{\partial s_w} \quad (4)$$

Here, ψ_w is the generation parameter for the thread surface of the hob cutter, and the matrices $\mathbf{M}_{hw}$ and $\mathbf{M}_{wc}$ are the coordinate transformation matrices between the coordinate systems. The matrices and model details can be found in [3].

For the sleeve of the coupling, the manufacturing process is shaper cutter generation, following the same steps defined for the hub. First, a hob cutter (Σ_s) is generated as a cutting tool based on the rack tooth surface (Σ_c) using the meshing equation (6). It follows a straight trajectory to determine the straight surfaces of the sleeve (Σ_g) as the envelope to the family of the shaper cutter surfaces. The coordinate transformation (5) from the coordinate system S_c to the coordinate system S_g, along with the consideration of the meshing equation (7) with the generation parameter ψ_s, allows to determine the sleeve tooth surface.

$$r_g(u, v, \psi_s, \phi_s) = \mathbf{M}_{gs}(\phi_s)\mathbf{M}_{sc}(\psi_s)\mathbf{r}_c(u, v) \quad (5)$$

$$f_4(u, v, \psi_s) = \left(\frac{\partial \mathbf{r}_s}{\partial u} \times \frac{\partial \mathbf{r}_s}{\partial v}\right)\frac{\partial \mathbf{r}_s}{\partial \psi_s} \quad (6)$$

$$f_5(u, v, \psi_s, \phi_s) = \left(\frac{\partial \mathbf{r}_g}{\partial u} \times \frac{\partial \mathbf{r}_g}{\partial v}\right)\frac{\partial \mathbf{r}_h}{\partial \phi_s} \quad (7)$$

Here, ϕ_s is the generation parameter for the sleeve surface, and the matrices $\mathbf{M}_{gs}$ and $\mathbf{M}_{sc}$ are the coordinate transformation matrices between the coordinate systems. The matrices and model details can be found in [3].

On the other hand, when experimentally validating the tooth root stress, the experimental geometry is measured using a coordinate measuring machine (CMM), from which the point cloud of the hub and sleeve tooth surfaces is extracted. The reconstruction of the surfaces is carried out using the methodology described in [4], which eliminates unnecessary points and generates an ordered point mesh suitable for the three-dimensional meshing required for subsequent finite element simulation.

2.2 Finite element model

To analyse the mechanical behaviour and contact trajectory of crowned gear couplings, the finite element method is employed. For this purpose, the method presented by Argyris et al. [31], commonly used for gear analysis, is employed to mesh the generated toothed surfaces. This well-known method produces a structured mesh on the gear teeth, dividing the surface into five sections: active profile, tooth root on the right and left sides, and the gear body. By analytically generating the tooth geometry using the model presented in the preceding section, the nodes forming the tooth surface are known. From these, the hexahedral element mesh is automatically generated inward for the hub and outward for the sleeve. Figure 1(a) shows a detail of the mesh used on the hub as an example. The element size is reduced in the potential contact region of the tooth, providing smaller elements in areas with higher stress gradients without increasing the number of elements and, therefore, the computational cost. As seen in Figure 1(a), the fine mesh zone corresponds to the region where contact will occur, which is defined by a contact analysis (TCA) [28], and an additional 25%. The element size gradually increases toward the edges of the coupling. Several layers of small elements ($l_{\min} = 0.08$ mm) characterized by thickness $e = 0.15$ mm [32] are generated on the tooth surface, which transition to larger elements in the body of the hub or sleeve.

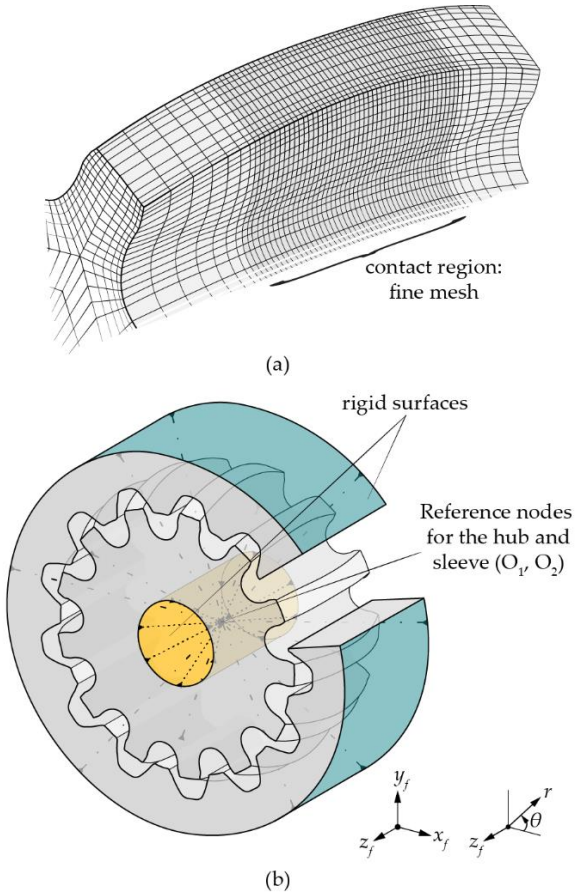

Fig. 1. (a) discretization of the longitudinal meshing of the finite element model with the identified contact zone, and (b) description of the boundary conditions and rigid surfaces defined in the finite element model (adapted from [17]).

The shaft and sleeve are assembled in a fixed coordinate system S_f. The auxiliary coordinate system S_m allows applying the misalignment angle by rotating the sleeve around the *x*-axis while keeping the hub fixed during the analysis. The origins of both coordinate systems are located at the central section of the coupling (0,0,0), where the reference nodes of the shaft and sleeve are also placed. These nodes are rigidly connected to the nodes located on the inner diameter of the hub and the outer diameter of the sleeve, respectively, to form rigid surfaces (shown in yellow and green in Figure 2(b)). Additionally, to perform the simulation and ensure proper post-processing of the data, a cylindrical coordinate system (r, θ, z_f) [17] is defined. During the simulation, the degrees of freedom of the sleeve are blocked, while in the hub, all degrees of freedom are blocked except for the rotation around the *z*-axis, allowing for the application of torque.

In these simulations, friction between the components is not taken into account, and contact is defined using node-to-segment contact pairs, with a tolerance equivalent to 1/20th of the smallest element size. Additionally, a linear elastic material is assumed (properties listed in Table 2), under the assumption that the deformations are small enough to be studied using the theory of small deformations. The selected element type is a first-order isoparametric hexahedral element (type 7 in the Marc simulation software [33]).

2.3 Test rig and experimental setup

For the experimental validation, [4] presents a specially designed static test rig to test crowned gear couplings with high misalignment angle ($\gamma_{max} = 10°$), which was used for this study. The test rig can be seen in Figure 2(a) and consists of two main parts: the static part, where the sleeve is placed and the torque is applied, and the movable part, where the hub is placed and the angular misalignment is applied in the clockwise direction. This is achieved using a pivoting system with a series of holes in the movable part and the base of the test rig, along with positioning pins, which allow for adjusting the angular misalignment degree by degree with an accuracy of $\pm 0.2°$. The torque is applied using calibrated weights up to a maximum of 1000 Nm and is measured using a full-bridge torque strain gauge (CEA-06-250US-350 by Micromeasurements), which was calibrated with a high-precision torque measurement unit to achieve an accuracy of ± 20 Nm.

The most commonly used method in the literature for empirical evaluation of the tooth root stresses is to use strain gauges [24,30,36]. Focusing on studies conducted on gear couplings, [34] numerically and experimentally analysed the load distribution along the length of the coupling, and [24] instrumented a tooth across the entire face width with miniature strain gauges. Quarter-bridge strain gauges and a data acquisition frequency of 100 Hz were used.

Therefore, in order to experimentally validate the stresses in the tooth root, based on the geometry of the coupling (properties in Table 2), all teeth except one will be machined to allow for proper attachment of the strain gauges and eliminate any convective effects from adjacent teeth. A quarter-bridge strain gauge (1-LY11-0.6/120 by HBM) with a wire width of 1 mm is placed on both sides of the tooth, as shown in Figure 2(b). These strain gauges allow for localized uniaxial strain measurements and can measure tension and compression caused by tooth bending.

The test conditions for the experiments are from 0 Nm to 150 Nm (since there is only a single tooth bearing the entire applied torque) and from 0° to 7° of angular misalignment, with five repetitions per test to ensure result repeatability and eliminate any clearance in the mechanism. Once the torque is applied using the calibrated weights, data acquisition is performed for 30 seconds to extract the average strain value for each strain gauge.

3 Results and Discussion

3.1 Experimental validation

In Figure 3, the results obtained from both the numerical model and the experimental tests are shown for different misalignment angles and as a function of the applied torque. The error bars displayed in each experimental data point represent the variability of the results obtained in all the repetitions conducted. Additionally, the shaded area represents the numerical values obtained within the torque precision range of $\Gamma \pm 20$ Nm, corresponding to the location of the strain gauge. The experimentally measured deformation values have been converted to stresses using

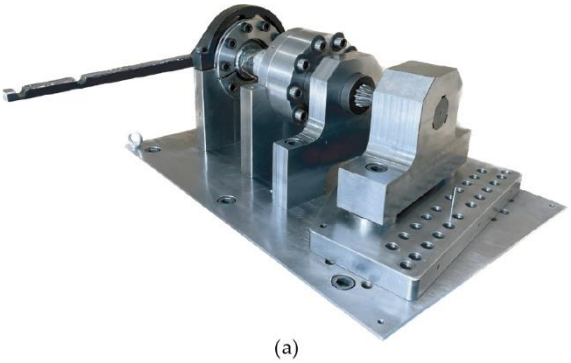

(a)

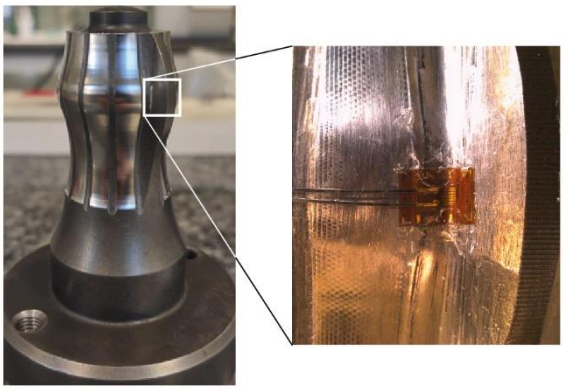

(b)

Fig. 2. (a) test rig designed [4] for conducting the experimental tests, and (b) machined coupling shaft with strain gauge used to measure bending deformations.

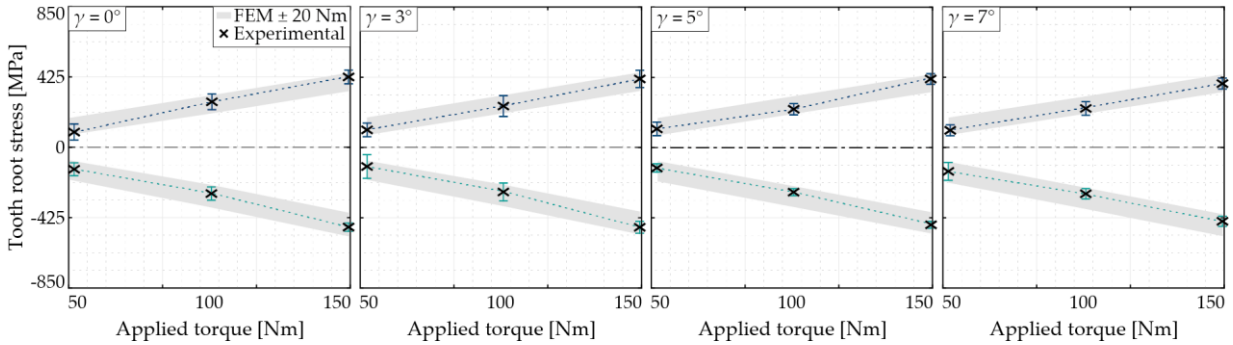

Fig. 3. Numerical-experimental comparison of tooth root stresses as a function of the applied torque for different misalignment angles.

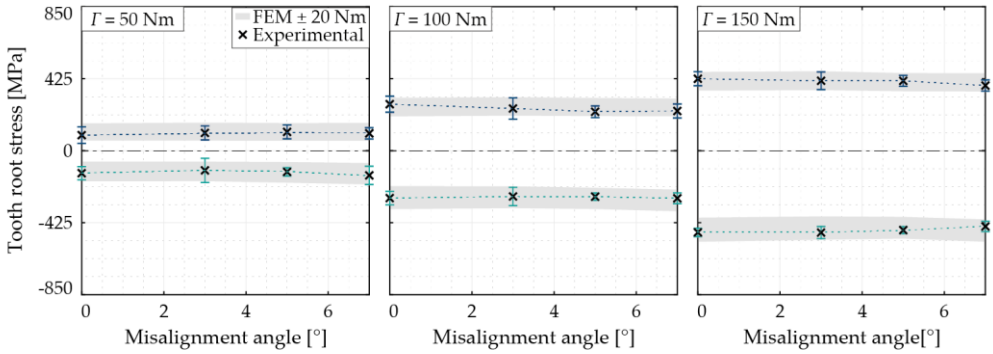

Fig. 4. Numerical-experimental comparison of tooth root stresses as a function of the misalignment angle for different applied torques.

the modulus of elasticity (Table 2): $\sigma = E\varepsilon$, to make the data more representative. As observed in the graphs, higher applied torques result in higher stresses at the tooth root. Additionally, compressive stresses are slightly higher than tensile stresses, consistent with the literature [35]. Furthermore, the experimentally obtained values fall within the range of the calculated numerical values. It should be noted that the observed differences could be attributed to variations while putting the gauges or the direction not being complete perpendicular to the tooth.

Furthermore, Figure 4 shows the evolution of tooth root stress in both the tension and compression sides, as a function of the misalignment angle for different applied torque values. The trend is similar for all torques, with the differences due to the influence of the misalignment angle becoming more significant at higher applied torques. The tooth root stress value does not vary significantly with the misalignment angle. This is because the stress is measured in a single tooth and single face width position. Therefore, the tooth root stress variation is only affected by the modification of the tooth stiffness caused by the displacement of the contact point.

This effect is better understood in Figure 5, which shows the normalized numerical tooth root stress values for different misalignment angles. The peak stress value shifts along with the contact point (Figure 5(a)), and the variation in the stress value does not exceed 10% (Figure 6(b-c)). Similarly, when looking at the stresses at the same point ($b = 0$ mm) for different misalignment angles (as done experimentally), the variation in stress is less than 20%. Experimentally, the differences are less pronounced due to the precision in the applied torque, the proximity between the contact points, and the error in the positioning of the strain gauges.

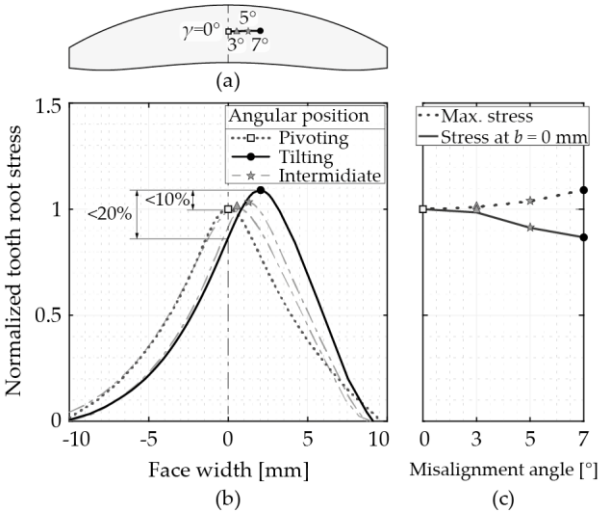

Fig. 5. Numerical results: (a) evolution of the contact point and (b) normalized tooth root stress as a function of the misalignment angle. (c) Variation of the normalized maximum tooth root stress as a function of the misalignment angle.

3.2 Methodology for the optimization of crowned gear coupling

As mentioned in Section 2, the described gear coupling in Table 2 is currently used in a high-strength steel rolling mill. Continuing with the coupling requirements specified in Table 1, this subsection identifies the optimal coupling geometry for this application using the models described in Sections 2.1-2.2.

Firstly, using the pre-design charts provided in [28], the parameters of the gear coupling geometry that can achieve a maximum angular misalignment of 6° are chosen. These charts are selected according to the desired pitch diameter,

in this case, 50 mm since it is the maximum allowed pitch diameter, and a smaller pitch radius would have a higher risk of tooth interference for high angular misalignments [28]. The charts also indicate the limits of undercut and pointed teeth, which should be avoided in a redesign as they weaken the life of the coupling. It is deduced that to achieve interference-free geometries that reach the desired misalignment, it is necessary to choose geometries with a reduced number of teeth or larger modules ($m = 5 - 6$ mm). Additionally, higher pressure angle allows achieving the desired angular misalignments without tooth interference or undercut. Based on these pre-design charts, the $\alpha = 20°$ geometries are discarded since tooth interference during the manufacturing process is inevitable to achieve the desired angular misalignment. Therefore, three geometries with $d_p = 50$ mm are selected, and three additional geometries with $d_p = 40$ mm (which matches the current coupling) to compare and decide which is the optimal geometry. The properties of the preselected geometries for the analysis are described in Table 3.

Table 3. Parameters of the preselected case studies numerically analysed.

	C 1	C 2	C 3	C 4	C 5	C 6
d_p, [mm]	50	50	50	40	40	40
m_n, [mm]	6	6	6	5	5	5
z, [-]	8	8	8	8	8	8
α, [-]	30	37.5	45	30	37.5	45
b/d_p, [-]	0.3	0.3	0.3	0.3	0.3	0.3
r_c, [mm]	24	27	27	20	20	23
Undercut	No	No	No	No	No	No
γ_{max}, [°]	6.7	7.2	8.5	6.6	8.2	8.3

After performing the simulation with the maximum misalignment angle ($\gamma = 6°$), the two parameters that influence the maximum stresses in the tooth are analyzed: the number of teeth in contact and the effective face width. Figure 6 shows the normalized number of teeth in contact and the normalized effective number of teeth in contact for each of the preselected cases. By solely considering the number of teeth in contact (Figure 6(a)), it is concluded that Case 4 is not suitable since it has the lowest number of teeth in contact for maximum misalignment, while Case 1 is the most appropriate. In other words, a larger pitch diameter with the same geometric properties of the teeth (except for the module in this case) provides a greater number of teeth in contact, resulting in lower tooth root stresses. However, previous studies [12,15,17,39] have shown that, due to the non-uniform load distribution in the presence of misalignment, the effective number of teeth in contact (Figure 6(b)) is a more relevant parameter for calculating the stresses in the tooth. In this comparison, it can be seen that there is not much variation in the results obtained among the analyzed cases. That is, all the chosen cases exhibit a similar load distribution, divided among approximately the same percentage of the tooth face width. This may be due to the low number of teeth in these geometries. Additionally, given the high degree of angular misalignment, even with an increase in the applied torque, the number of teeth in contact does not increase.

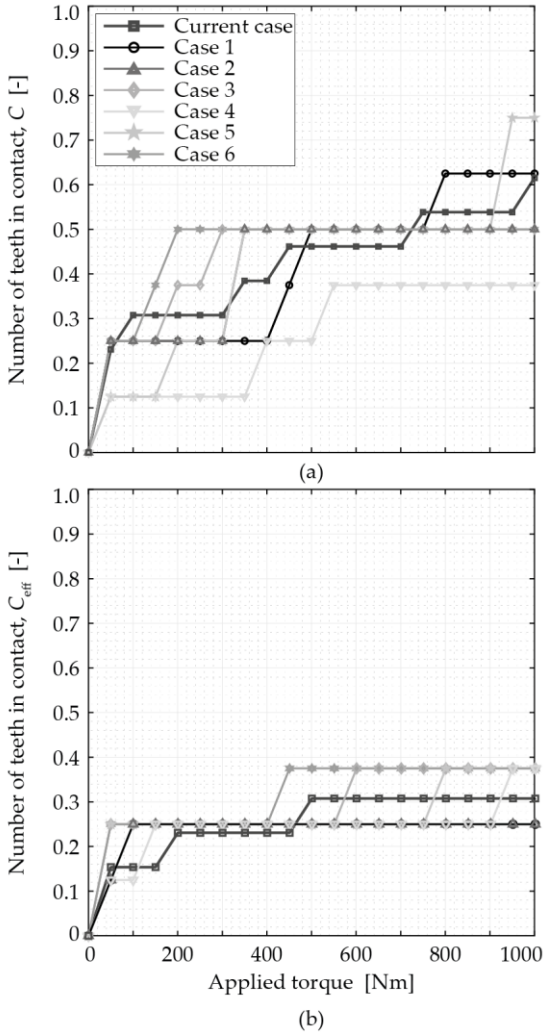

Fig. 6. (a) number of teeth in contact and (b) number of teeth in effective contact normalized for the preselected cases as a function of applied torque.

On the other hand, Figure 7 shows the effective face width calculated from the simulation results. It can be observed that, for the same aspect ratio, the effective face width is greater in cases with a smaller pitch diameter ($d_p = 40$ mm). This means that having a larger face width does not necessarily mean that this width is bearing the load. Cases 4, 5, and 6 have an effective face width of approximately 75% of the total length of the coupling, while cases 1, 2, 3, and the current case have a 50% effective face width. This indicates that cases 4, 5, and 6 are more optimized compared to the current case, as they have a larger tooth width supporting the load. No effect of the pressure angle on the effective face width is observed. In Figure 8, the stress distribution in the tooth for the maximum applied torque ($\Gamma = 500$ Nm) with an angular misalignment of $\gamma = 6°$ can be seen. There is a difference between the current case and the rest of the generated cases in terms of the position of the maximum stress value position (corresponding to the contact point). The parameter that influences this is the crowning radius,

which is 10 mm in the current case and between 20-27 mm for the other generated cases. A smaller crowning radius for the same angular misalignment results in the contact being more centred on the tooth width. However, reducing the crowning radius increases the risk of interference during manufacturing. It can be observed that the influence of the pitch diameter on the stresses is less pronounced with higher pressure angles. Lower stresses are obtained with $\alpha = 45°$ due to the greater tooth thickness.

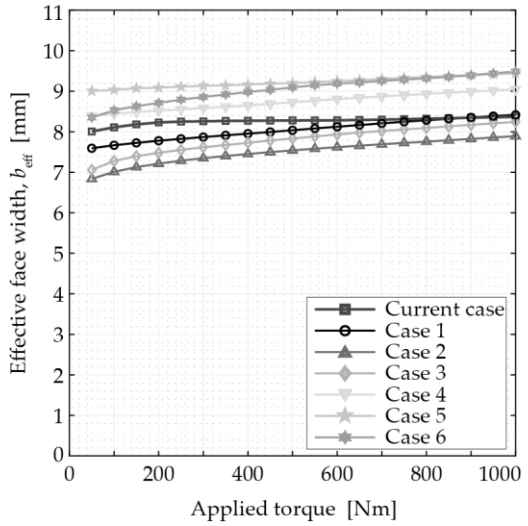

Fig. 7. Effective face width as a function of applied torque.

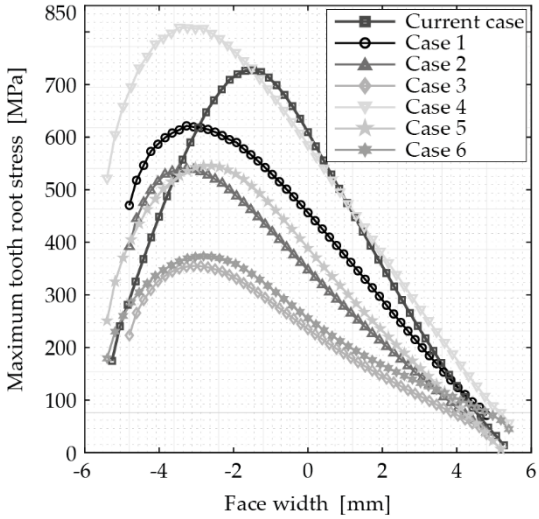

Fig. 8. Maximum stress in the tooth along the face width for the preselected cases and an angular misalignment of $\gamma = 6°$.

After analyzing the two main parameters influencing the stress in the tooth, Figure 9 shows the evolution of the maximum tooth root stress as a function of the applied torque. A higher pressure angle results in a reduction of stress of over 50% compared to the current case. This reduction is primarily due to the increased tooth thickness provided by the coupling manufactured with $\alpha = 45°$, as the influence on the number of teeth in contact is not evident. Additionally, it has been observed that a larger primitive diameter does not offer remarkable advantages in the analyzed case. Indeed, the stresses are higher despite having a wider face width to bear them, in cases with a smaller pitch diameter.

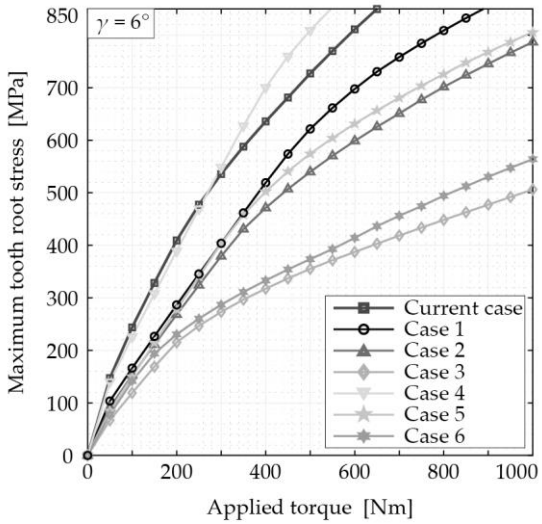

Fig. 9. Maximum stress in the tooth for the preselected cases as a function of applied torque for $\gamma = 6°$.

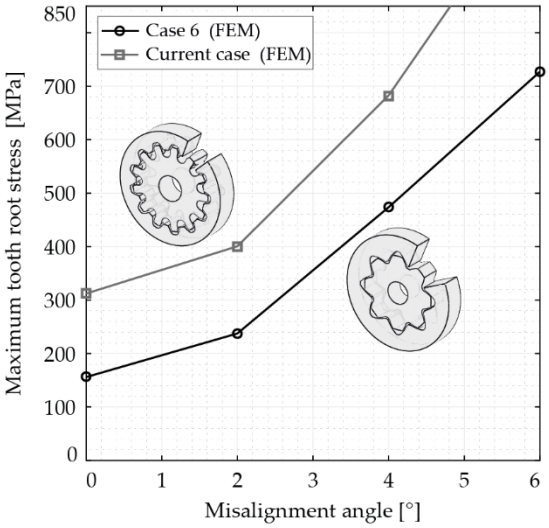

Fig. 10. Numerical-analytical maximum stress in the tooth for the Current Case and the optimized case (Case 6) as a function of the misalignment angle $\Gamma = 1000$ Nm.

Therefore, to conclude that case 6 is suitable for improving the current employed geometry, Figure 10 shows the evolution of the maximum tooth root stress as a function of the misalignment angle for the maximum applied torque. A reduction of approximately 50% in stress is confirmed across the entire range of misalignment angles. Thus, with the optimized design, it would be possible to increase the torque applied to the rollers or increase the lifespan of the couplings, even at the highest misalignment angle.

4 Conclusions

This work shows a compilation of analytical and numerical models for the determination and calculation of tooth root stresses in crowned gear couplings working in high misalignment applications. It experimentally validates the numerically obtained stresses and proposes a methodology to optimize existing designs or even to realize new designs. The results obtained show the effectiveness of the numerical models, proposing a design with which it is possible to reduce the tooth root stresses by more than 50%. This change will extend the useful life of the component, as well as increase the maximum applicable torque. All of these are advantages for the user, manufacturer or seller of the rolling machine.

It has been shown that the effective number of teeth in contact is a key parameter to determine the tooth root stress and that it has little to do with the number of teeth in contact. Furthermore, it is concluded that the pressure angle has a great influence on the reduction of tooth root stresses in gear couplings working in high misalignment angles. Likewise, it has been found that the effective face width does not vary excessively among the cases analysed herein.

References

1. S. Hahn, *Encyclopedia of Automotive Engineering* (2014)
2. M. Alfares et al., Mech. Mach. Theory **41** (10) (2006)
3. A. Iñurritegui et al., Mech. Mach. Theory **164** (2021)
4. A. Iñurritegui et al., Mech. Mach. Theory **183** (2023)
5. Y. Guan, et al., Mech. Mach. Theory **136** (2019)
6. F. Ohshima, et al., *Trans. Jpn. Soc. Mech. Eng. C* **78** (786) (2012)
7. AGMA 945-1-B20, "Splines – Design and Application", American Gear Manufacturers Association, 2020
8. G. Henriot, et al., *Accouplements, alignement des axes, Engrenages : Conception, Fabrication, Mise en œuvre* (1983)
9. R. Cedoz, et al., *Society of Automotive Engineers* (1994)
10. ISO 21771, "Gears-Cylindrical Involute Gears and Gear Pairs-Concepts and Geometry", International Organization for Standardization, 2007
11. Y. Guan, et al., Mech. Mach. Theory **126** (2018)
12. B. de Caires, PhD thesis, *Brigham Young University* (2006)
13. Y. Guan, et al., J. Mech. Eng. Sci. (2018)
14. S. Medina, et al., J. Tribol. **124** (2) (2002)
15. J. Silvers, et al., *Proceeding of the FTM* (2010)
16. F. Curà, et al., Proc. Inst. Mech. Eng., Part C **227** (10) (2013)
17. A. Iñurritegui, et al., Mech. Mach. Theory **179** (2023)
18. K. Nakashima, *Trans. Jpn. Soc. Mech. Eng. C* **502** (54) (1988)
19. D. Dudley, Prod. Eng. **28** (1957)
20. ISO 4156, "Straight Cylindrical Involute Splines", International Organization for Standardization, 2005
21. J. Larrañaga, et al., *Proceedings of the 5th Inter. Conf. Power Transmission-BAPT* (2016)
22. Y. Guo, et al., Mech. Mach. Theory **98** (2016)
23. V. Cuffaro, et al., Proc. Inst. Mech. Eng., Part C **226** (12) (2012)
24. M. Benatar, et al., J. Adv. Mech. Des. **11** (6) (2017)
25. Y. Guan, et al., J. Adv. Mech. Des. **5** (2021)
26. V. Cuffaro, et al., Key Engineering Materials (2014)
27. J.R. Mancuso, *Technology & Engineering* (1986)
28. A. Iñurritegui, et al., Mech. Mach. Theory **173** (2022)
29. W. Herbstritt, et al., Iron Steel Eng. **76** (7) (1999)
30. F. Litvin, et al., *Gear Geometry and Applied Theory* (2004)
31. J. Argyris, et al., Comput. Methods Appl. Mech. Eng. **191** (11–12) (2002)
32. I. Gonzalez-Perez, et al., Transactions of ASME, J. Mech. Des. **140** (2) (2017)
33. MSC.Software, Marc 2019 - Volume B: Element Library (2019)
34. D. Petersen, PhD thesis, *TIB Hannover* (1989)
35. DIN 5466, "Splined joints, calculation of load capacity", Deutsche Institut für Normung, 2002